

## Article

# TD-DFT Monitoring of the Absorption Spectra of Polycyclic Aromatic Hydrocarbons over the Basque Country, Spain

Patricia González-Berdullas <sup>1</sup>  and Luís Pinto da Silva <sup>1,2,\*</sup> 

<sup>1</sup> Chemistry Research Unit (CIQUP), Faculty of Sciences of University of Porto (FCUP), R. Campo Alegre 697, 4169-007 Porto, Portugal; patricia.berdullas@fc.up.pt

<sup>2</sup> LACOMEPII, GreenUPorto, Department of Geosciences, Environment and Territorial Planning, Faculty of Sciences of University of Porto, R. Campo Alegre 697, 4169-007 Porto, Portugal

\* Correspondence: luis.silva@fc.up.pt

**Abstract:** Brown carbon is a type of carbonaceous aerosol with strong light absorption in the ultraviolet and visible wavelengths that leads to radiative forcing. However, it is difficult to correlate the chemical composition of brown carbon with its atmospheric light absorption properties, which translates into significant uncertainty. Thus, a time-dependent density functional theory (TD-DFT) approach was used to model the real-world absorption properties of 14 polycyclic aromatic hydrocarbons (PAHs) over three regions of the Basque Country (Spain): Bilbao, Urretxu, and Azpeitia. The data were corrected for atmospheric concentration. The results show that the absorption spectra over each region are qualitatively identical, with the absorption intensities being significantly higher over Bilbao than over Azpeitia and Urretxu. Furthermore, it was found that the light absorption by PAHs should be more relevant for radiative forcing when it occurs at UVA and (sub)visible wavelengths. Finally, among the 14 studied PAHs, benzo[*b*]fluoranthene, pyrene, fluoranthene, benzo[*a*]pyrene, and benzo[*k*]fluoranthene and benzoperylene were identified as the molecules with larger contributions to radiative forcing.

**Keywords:** brown carbon; polycyclic aromatic hydrocarbons; radiative forcing; absorption spectra; density functional theory; organic aerosols



**Citation:** González-Berdullas, P.; Pinto da Silva, L. TD-DFT Monitoring of the Absorption Spectra of Polycyclic Aromatic Hydrocarbons over the Basque Country, Spain. *Sustain. Chem.* **2021**, *2*, 599–609. <https://doi.org/10.3390/suschem2040033>

Academic Editor: Ivano Alessandri

Received: 13 September 2021

Accepted: 23 October 2021

Published: 29 October 2021

**Publisher's Note:** MDPI stays neutral with regard to jurisdictional claims in published maps and institutional affiliations.



**Copyright:** © 2021 by the authors. Licensee MDPI, Basel, Switzerland. This article is an open access article distributed under the terms and conditions of the Creative Commons Attribution (CC BY) license (<https://creativecommons.org/licenses/by/4.0/>).

## 1. Introduction

Light-absorbing aerosols have been receiving significant attention during the past few years, due to the increasing realization of their important role in radiative forcing [1–4]. A large proportion of this type of aerosol is composed of carbonaceous components, such as black carbon (BC) and brown carbon (BrC) [2,5]. While BC is known to be an important absorber due to its strong light absorption, the properties and importance of BrC are still poorly understood.

Absorption of solar radiation by BrC in the ultraviolet (UV) and (sub)visible wavelengths accounts for ~20–40% of aerosol absorption at 350 nm and 27% at 404 nm (absorption at 536 nm is negligible) [6–8]. Some authors even state that BrC dominates absorption by aerosols at specific wavelengths and/or specific regions of the globe [9,10]. While the mass absorption of BrC can be lower than that of BC, UV absorption by carbonaceous aerosols becomes relevant due to its sheer abundance in continental aerosols [5]. Despite this, many climate models still downplay the contribution of BrC to light absorption [10,11], which could explain why there are still significant differences between model predictions of aerosol-related radiative forcing and real measurements [3,12].

Understanding the photophysics of BrC aerosols is essential for the accurate modeling of radiative forcing. However, quantitatively predicting the contribution of BrC aerosol to light absorption is not trivial: while the optical properties of organic compounds depend on their molecular structures, there is a lack of detailed information on the composition of BrC and its impact on absorption spectra [3,13]. BrC aerosols, which can also

be generated by atmospheric processes such as oxidation and solar irradiation [11,14,15], are composed of diverse structures with different light-absorption properties: polycyclic aromatics (and their oxygenated and nitrated derivatives), phenols, biopolymers, or humic-like substances [2,16,17]. Furthermore, both the concentration and composition of BrC can change significantly across emission locations and sources [3,13]. Online (real-time) light absorption measurements of BrC are complex, and the results differ from those provided by offline methods (e.g., solvent extraction of pollutants) [18].

Despite such uncertainties, polycyclic aromatic hydrocarbons (PAHs) have been identified as ubiquitous compounds [19], act as important chromophores in BrC [4,5,8,20], and are among the most recurrent environmental contaminants, being classified as persistent environmental pollutants [21,22]. While PAHs can be emitted into the atmosphere in natural burning events, the main contribution comes from anthropogenic sources, such as motor vehicle exhaust, coal burning, and industrial activities [23].

Obtaining reliable atmospheric light absorption measurements of PAHs is important for understanding and predicting the radiative forcing effect of BrC aerosols. Herein, this study aims to use a computational chemistry approach to model the real-world absorption spectra of atmospheric PAHs by considering their experimental atmospheric concentration and speciation. This approach can determine which PAHs have higher radiative forcing potential: the most relevant regions in their UV and visible spectra are identified in terms of radiative forcing, and their light absorption is correlated to individual species. The obtained data will be invaluable for the prediction of real-world light absorption measurements of BrC aerosols over different regions of the globe, which is essential for the development of accurate global models to predict and mitigate the radiative forcing effects of BrC.

Modeling efforts rely on a density functional theory (DFT) approach, which has been increasingly and successfully used in the field of environmental sciences, for example, to determine reaction mechanisms and energetics in systems and reactions of environmental concern [24–27]. Besides providing reliable results, DFT calculations present some advantages over experimental studies since they do not require a large number of steps, as is the case in chemical synthesis, separation/purification, and characterization. DFT can also be extended to account for the time-dependent (TD) nature of electromagnetic waves and used to model excited states [28]. DFT calculations are also the most widely used approach to model the structure, photophysics, and photochemistry of organic molecules, including BrC [29–32].

The developed model is based on the speciation and quantification of PAHs over the atmosphere of three regions of the Basque Country, an autonomous region in Northern Spain. One dataset was provided by the work of Elorduy et al., who collected PM<sub>10</sub> samples between July and December 2013 in an urban area of the city of Bilbao [33]. The other dataset was provided by the work of Oleagoitia et al., who collected PM<sub>2.5</sub> samples between October 2011 and October 2012 in Azpeitia and Urretxu, two villages in Gipuzkoa, an area characterized by an industrial sector focused on iron and steel [34]. The former study identified 13 PAHs (mean concentration of 0.06–0.69 ng m<sup>-3</sup>), while the latter identified 11 PAHs (mean concentration of 0.05–0.19 ng m<sup>-3</sup>) (Table S1, Supplementary Materials).

Our group previously used a similar computational approach to model the real-world absorption spectra of PAHs over the atmosphere of four cities: Porto (Portugal), Florence (Italy), Athens (Greece), and Seoul (South Korea) [35,36], and concluded that in all cities, PAHs should contribute to radiative forcing mainly through light absorption in the UVB/UVA region of the spectrum, but also moderate light absorption in the blue region of the visible spectrum. PAHs such as fluoranthene, benzo[*a*]anthracene, dibenzo[*a,h*]anthracene, and coronene were identified as main contributors to UV absorption, while PAHs such as benzoperylene, benzo[*a*]pyrene, and indenopyrene as capable of visible light absorption. Interestingly, our calculations identified Porto as the most affected by PAH-induced radiative forcing among the studied cities. By expanding this modeling effort to more regions of the world, we expect to develop a more comprehensive and global

assessment of the effect of PAHs on radiative forcing, which is needed in order to develop more global climate models, including BrC aerosols.

## 2. Computational Methods

For this study, 14 PAHs (naphthalene (NAP), phenanthrene (PHE), fluoranthene (FLUO), pyrene (PYR), benzo[*a*]anthracene (BaA), chrysene (CHRY), benzo[*b*]fluoranthene (BbF), benzo[*k*]fluoranthene (BkF), benzo[*a*]pyrene (BaP), benzoperylene (BghiP), indeno[1,2,3-*cd*]pyrene (IdP), fluorene (FLU), dibenzo[*a,h*]anthracene (DahA) and anthracene (ANTH)) (Figure S1) were computed and then corrected with their experimental atmospheric concentrations over three Basque Country regions (Table S1), which were extracted from the works of Elorduy et al. and Oleagoitia et al. [33,34].

The present calculations were performed with the Gaussian 09 program package [37] at two levels of theory. All calculations were made in the gas phase. Calculations were performed with stable wavefunctions with a closed-shell approach. First, the geometries of each PAH were optimized by using the PBE0 density functional [38] and the 6-31G(d,p) basis set, while vibrational calculations were made at the same level of theory to ensure that the obtained structures were at the minima in their potential energy surface. This functional was chosen because it provides accurate geometric optimization of organic molecules [39–42].

The absorption properties (oscillator strength and absorption wavelengths) were calculated by performing single-point vertical excitation calculations with a TD-DFT approach, by computing 10 singlet excited states on top of the structures obtained at the PBE0/6-31G(d,p) level of theory. These single-point calculations were performed with a 6-31+G(d,p) basis and 4 density functionals: BP86, PBE0, B3LYP, and  $\omega$ B97XD. BP86 is a generalized gradient approximation (GGA) functional composed of the Becke 1988 and Perdew 86 correlation functionals [43]. BP86 was previously used in the study of the real-world absorption spectra of PAHs (and derivatives) over different locations of the globe [35,36]. PBE0 is a hybrid functional that mixes the Perdew–Burke–Ernzerhof (PBE) exchange energy and Hartree–Fock exchange energy, along with full PBE correlation energy [38]. B3LYP is another hybrid functional, which uses the non-local correlation provided by the Lee–Yang–Parr (LYP) expression and VWN functional III for local correlation [43]. Finally,  $\omega$ B97XD is a long-range-corrected hybrid functional that includes empirical dispersion [44]. PBE0 and B3LYP generally provide accurate estimates for local  $n \rightarrow \pi^*$  and  $\pi \rightarrow \pi^*$  states, while functionals such as  $\omega$ B97XD are typically required for either charge-transfer (CT) or Rydberg transitions [28].

The absorption spectrum for individual PAH species was plotted with SpecDis software (version 1.71) [45], based on the 10 singlet excited state transitions calculated at the TD (BP86, PBE0, B3LYP, or  $\omega$ B97XD)/6-31+G(d,p) level of theory. The curves were generated with a Gaussian band shape and a peak broadening of 0.16 eV. The combined theoretical absorption spectrum of all PAHs was obtained by summing the individual spectra, without considering the experimentally obtained concentrations, resulting in absorption intensities only composed by  $\epsilon$  ( $\text{mol}^{-1} \text{cm}^{-1}$ ) [45]. The next step was to correct the intensity values of this spectrum by considering the experimentally obtained concentrations of target PAHs for each of the three Basque Country regions, which was achieved by multiplying the theoretical absorption intensity ( $\epsilon$ ) of each PAH by its atmospheric concentration ( $\text{ng m}^{-3}$ ), resulting in absorption intensities expressed as absorption per concentration ( $\epsilon \times \text{ng m}^{-3}$ ). The global spectrum was obtained as the sum of individual spectra.

This computational approach was successfully used by our group to model the real-world absorption spectra of different PAH datasets present in the atmosphere over different regions in Europe and Asia [35,36].

## 3. Discussion and Results

The combined absorption spectra of the PAHs found over different regions of Basque Country (Spain), when calculated with BP86 and corrected for their mean experimental

concentrations, are presented in Figure 1. The absorption spectrum over Azpeitia consists of two stronger peaks at  $\sim 300$  and  $\sim 330$  nm (UVB and UVA regions); three peaks of more moderate intensity at  $\sim 220$ ,  $\sim 230$ , and  $\sim 425$  nm (UVC and visible regions); and a weaker band at  $\sim 380$  nm (UVA region). The absorption spectrum for Urretxu, the other location in the Gipuzkoa region, is identical to that found for Azpeitia. Nevertheless, we can see the decrease of relative importance of the peak at  $\sim 230$  nm and the appearance of small shoulders at  $\sim 250$  and  $\sim 265$  nm. Interestingly, the major difference between the absorption spectra of the two Gipuzkoa locations may be their intensity, which is higher in Azpeitia than in Urretxu. This indicates that these PAHs could lead to higher radiative forcing effects in the former than in the latter, which is not unexpected, given that the mean concentration of PAHs is slightly higher over Azpeitia ( $0.90 \text{ ng m}^{-3}$ ) than over Urretxu ( $0.73 \text{ ng m}^{-3}$ ), as seen in Table S1. Regarding Bilbao, the most notable difference between its related absorption spectrum and the spectra for the Gipuzkoa region (Figure 1) is also the absorption intensity. More specifically, while the maximum absorption intensity is just  $\sim 10,000\text{--}12,000 \text{ e} \times \text{ng m}^{-3}$  in the latter region, in Bilbao the maximum absorption is about six times higher ( $\sim 60,000 \text{ e} \times \text{ng m}^{-3}$ ). Thus, Bilbao should be subjected to significantly more PAH-induced radiative forcing than the Gipuzkoa region. Once again, this is not unexpected, as the mean concentration of PAHs over Bilbao ( $3.29 \text{ ng m}^{-3}$ ) is higher than in Azpeitia and Urretxu ( $0.79\text{--}0.90 \text{ ng m}^{-3}$ ) [33,34]. What is interesting is that the difference between absorption intensities is about six times higher than the difference between mean concentrations (about 3.5–4.5 times). Thus, the contribution of PAHs to radiative forcing in certain locations/regions could be more problematic than expected if we just consider the obtained mean concentrations.

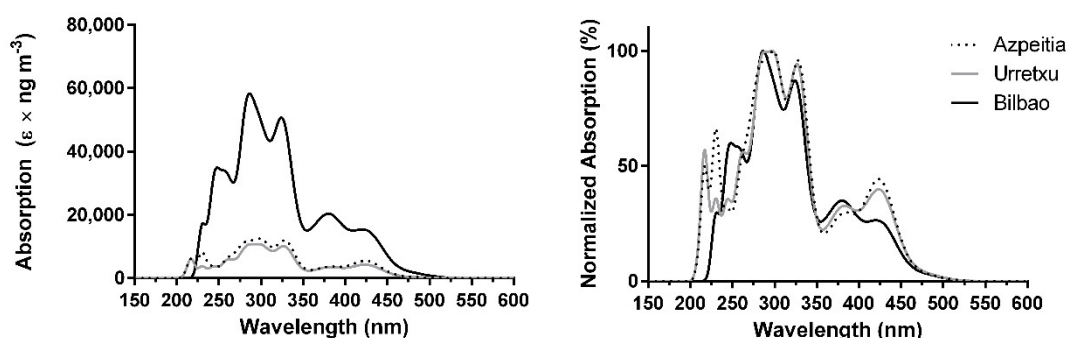


**Figure 1.** Combined theoretical absorption spectra of PAHs, corrected for their experimental mean concentrations, over Azpeitia, Urretxu, and Bilbao using BP86/6-31+G(d,p) [33,34]. (left) absolute values; (right) normalized values.

As for the concentration-corrected absorption spectra, computed at the TD PBE0/6-31+G(d,p) level of theory, the results can be found in Figure 2. The spectra are qualitatively identical among the three locations, being composed of three stronger bands at  $\sim 270$ ,  $\sim 255$ , and  $\sim 300$  nm (UVC and UVB regions); three moderate bands at  $\sim 345$ ,  $\sim 400$ , and  $\sim 235$  nm (UVA, UVC, and a small extent of the visible region); and a weaker band at  $\sim 215$  nm (UVC region). Thus, these results indicate that PBE0 predicts an absorption spectrum more blue-shifted (Figure 2) than that generated with BP86 (Figure 1). That is, light absorption is more intense in the UVC-UVB than the UVB-UVA range. There are no other major qualitative differences between the spectra calculated with the two methods. In terms of intensity difference, PBE0 also predicts similar absorption intensity over the Gipuzkoa region, with the absorption over Bilbao being significantly higher. Furthermore, the difference in absorption intensity between Bilbao and the Gipuzkoa region (4–5 times) is still higher than the simple difference in atmospheric concentration of PAHs (about 3.5–4.5 times).

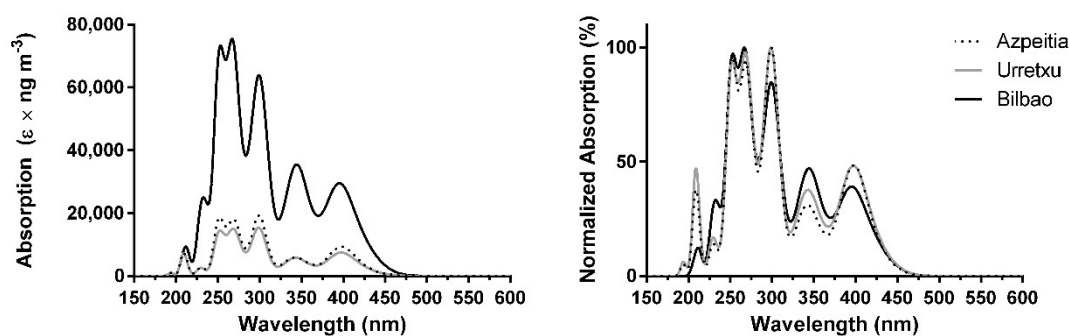


**Figure 2.** Combined theoretical absorption spectra of PAHs, corrected for their experimental mean concentrations, over Azpeitia, Urretxu, and Bilbao using PBE0/6-31G(d,p) [33,34]. (**left**) absolute values; (**right**) normalized values.

The absorption spectra, computed with the B3LYP functional and corrected for the experimental concentration of PAHs, can be found in Figure 3. The results are similar to those obtained with PBE0 (Figure 2) and BP86 (Figure 1), with some differences. The two stronger peaks (which are somewhat mixed) are at  $\sim 265$  and  $\sim 270$  nm (UVC region), followed by two relevant bands at  $\sim 240$  and  $\sim 305$  nm (UVC and UVB regions). Another moderate band can be found at  $\sim 360$  nm (UVA region), with a weaker band in the visible region ( $\sim 415$  nm). These results can be considered as somewhat intermediate compared to those obtained with PBE0 and BP86, as the results obtained with B3LYP (Figure 3) are red-shifted compared to those obtained with PBE0 (Figure 2), and not as red-shifted as BP86 (Figure 1). The absorption intensity over Bilbao is once again 4–5 times higher than in the Gipuzkoa region.

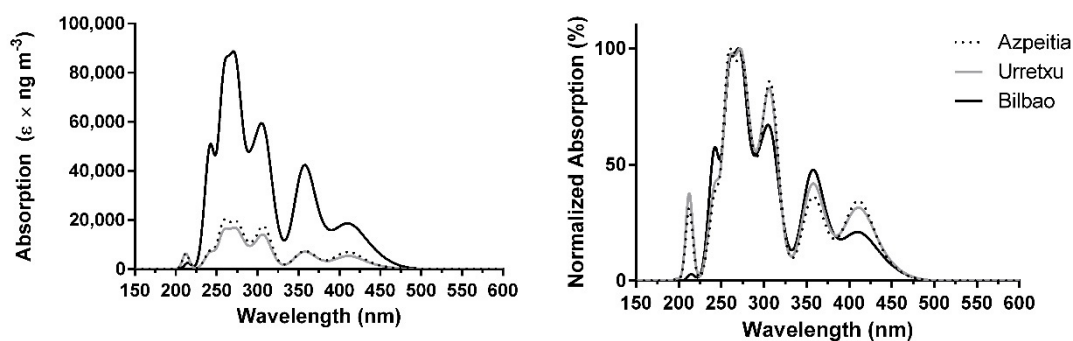


**Figure 3.** Combined theoretical absorption spectra of PAHs, corrected for their experimental mean concentrations, over Azpeitia, Urretxu, and Bilbao using B3LYP/6-31+G(d,p) [33,34]. (**left**) absolute values; (**right**) normalized values.

Finally, the absorption spectra computed at the TD  $\omega$ B97XD/6-31+G(d,p) level of theory, when corrected for the mean atmospheric concentration of the studied PAHs, can be found in Figure 4. This functional provides the most blue-shifted results, with the spectra being composed of two stronger bands at  $\sim 245$  and  $\sim 215$  nm (UVC region), followed by moderate absorption at  $\sim 275$  and  $\sim 325$  nm, and a weaker absorption band can be found at  $\sim 380$  nm (Bilbao) and  $\sim 365$  nm (Gipuzkoa region). Once again, the difference in intensity between Bilbao and the Gipuzkoa region is 4–5 times.

It should be noted that while the absorption intensity of PAHs over Bilbao was found to be significantly higher than over Azpeitia/Urretxu, it is still significantly lower compared to other important Southern European cities. While the maximum light absorption intensity found for Bilbao was  $60,000 \text{ e} \times \text{ng m}^{-3}$  (with BP86, Figure 1), the same functional calculated an absorption intensity maxima of  $\sim 100,000$ – $400,000 \text{ e} \times \text{ng m}^{-3}$  for Porto (Portugal), Florence (Italy), and Athens (Greece) [36]. This indicates that Bilbao is still relatively protected from PAH-induced radiative forcing, at least when compared with other Southern European cities.

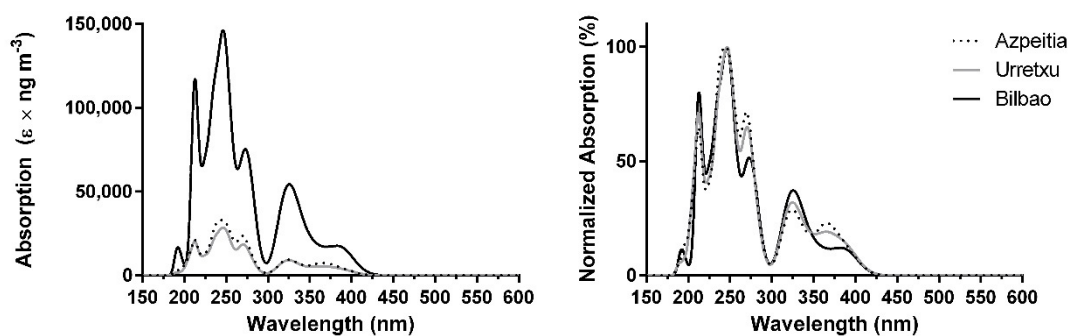


**Figure 4.** Combined theoretical absorption spectra of PAHs, corrected for their experimental mean concentrations, over Azpeitia, Urretxu, and Bilbao using  $\omega$ B97XD/6-31+G(d,p) [33,34]. (left) absolute values; (right) normalized values.

In summary, the absorption spectra of PAHs are qualitatively similar for all locations (Bilbao, Azpeitia, and Urretxu) regardless of the employed functional, with the absorption intensities being similar in the Gipuzkoa region but significantly lower than in Bilbao. The main difference is the position in the bands. Figure 5 presents the normalized absorption spectrum over Bilbao (as a representative example) calculated with all functionals. We can see that the number and shape of the bands are similar, with each functional simply shifting the maximum wavelength. For example, we can see that the band computed by  $\omega$ B97XD at  $\sim 380$  nm corresponds to the band found at  $\sim 400$ – $425$  nm (Figure 5). Similarly, the bands found at  $\sim 380$  (BP86),  $\sim 360$  (B3LYP),  $\sim 345$  (PBE0), and  $\sim 325$  nm ( $\omega$ B97XD) should correspond to the same maximum wavelength (Figure 5). The bands at  $\sim 330$  (BP86),  $\sim 305$  (B3LYP),  $\sim 300$  (PBE0), and  $\sim 275$  nm ( $\omega$ B97XD) should correspond to the same band in the real-world absorption spectra. The same can also be said for the bands found in the UVC region. Given these data, there is general agreement between the calculations with different functionals that stronger light absorption occurs in the UVC and UVB regions, with more moderate absorption in the UVA region and weaker absorption in the visible region.

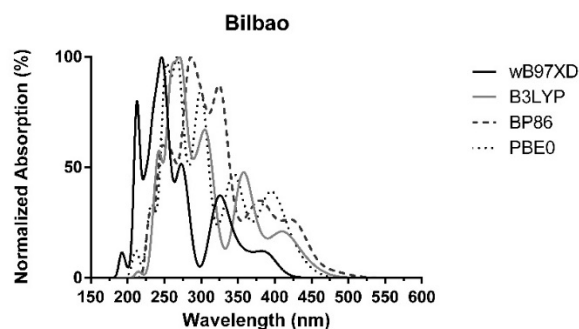


**Figure 5.** Normalized combined theoretical absorption spectra of PAHs, corrected for their experimental mean concentrations over Bilbao, using BP86/6-31+G(d,p), PBE0/6-31G(d,p), B3LYP/6-31+G(d,p), and  $\omega$ B97XD/6-31+G(d,p) [33,34].

At this point of the study, it is important to note that UVC radiation is completely filtered by the atmosphere. Moreover, not much ground-level solar insolation at  $\sim 290$ – $300$  nm is expected due to ozone absorption [46]. Thus, the only bands that should be relevant for PAH-induced radiative forcing are those with wavelengths above that threshold:  $\sim 330$ ,  $\sim 385$ , and  $\sim 425$  nm for BP86;  $\sim 345$  and  $\sim 400$  nm for PBE0;  $\sim 305$ ,  $\sim 360$  and  $\sim 415$  nm for B3LYP; and  $\sim 325$  and  $\sim 365$ – $380$  nm for  $\omega$ B97XD. We can see that there is qualitative agreement between all functionals. The results are also in line with BrC-related measurements. More specifically, it was reported that BrC contributes  $\sim 20$ – $40\%$  to aerosol absorption at  $350$  nm and  $27\%$  at  $404$  nm, with almost negligible absorption at  $536$  nm [6–8]. These values are in line with the absorption bands found at  $\sim 330$ – $385$  and  $\sim 400$ – $425$  nm predicted here (Figures 2–4). These reported values also indicate that  $\omega$ B97XD excessively blue-shifts the

absorption spectra, while the other functionals predict light absorption at wavelengths more closely related to BrC measurements.

Subsequently, the next step of the study was to decompose the absorption intensity of the bands referred to above into the relative contribution of individual PAHs (Tables S2–S9). It should be noted that we excluded the absorption band found at ~330 nm for BP86, as it appeared to correspond to the bands found at ~275–305 nm for other methods.

Starting with calculations made with the BP86 functional, the contributions of PAHs to light absorption at ~380 nm (as predicted by BP86) can be found in Table S2. BbF is the major contributor in all cases (51–58%), followed to a lesser extent by FLUO (16–21%), PYR (7–14%), and IdP (7–11%). The relative contributions to absorption at ~425 nm (computed with BP86) can be found in Table S3. Once again, there is a major contributor to the absorption intensity at this wavelength: BghiP (30–60%), and its contribution is significantly higher in Azpeitia/Urretxu (49–60%) than in Bilbao (30%). BaP, BkF, and IdP are also relevant contributors at similar levels in all locations.

As for the PBE0-related results, the individual contributions of PAHs to light absorption at ~345 nm can be found in Table S4. The results are quite similar in all locations, with 96% of light absorption being explained by contributions from BbF (31–41%), PYR (26–32%), CHRY (15–16%), and FLUO (13–17%). As for light absorption at ~400 nm (Table S5), the most relevant contributions are from BghiP (22–50%), BbF (23–37%), BkF (12–19%), and BaP (9–11%). Interestingly, while in the Gipuzkoa region BghiP is clearly dominant (40–50%), in Bilbao it is not (22%). In the latter region, BbF is clearly dominant (37%), while it shows more moderate contributions in Azpeitia/Urretxu (23–27%).

The individual contributions of PAHs (as computed with B3LYP) to absorption at ~360 nm can be found in Table S6. The results are very similar to those computed with PBE0 (Table S4), with light absorption being explained mainly by contributions from BbF (42–49%), PYR (23–28%), FLUO (13–15%), and CHRY (10%). The main difference between B3LYP and PBE0 is that the former predicts higher contributions from BbF than the latter, with varying decreased contributions of the other PAHs. In terms of the contributions to absorption at ~410 nm (Table S7), B3LYP predicts that the main contributors are BghiP (34–54%), BkF (15–27%), BaP (15–23%), and BaA (4–7%). Once again, BghiP is dominant in Azpeitia/Urretxu (53–64%), while in Bilbao its contribution (34%) is similar to that of BkF (27%).

Finally, the decomposition of light absorption at ~325 nm into individual contributions from PAHs (for  $\omega$ B97XD) can be found in Table S8. Here, the main contributors are BbF (44–53%), PYR (18–23%), FLUO (14–16%), and CHRY (8%). As for the contributions to light absorption at ~365–380 nm (Table S9), the main contributors are BghiP (21–75%), BaP (9–53%), BkF (1–12%), BaA (2–8%), and IdP (3–19%). Interestingly, at this wavelength, the  $\omega$ B97XD functional predicts major differences between locations. For one, while BghiP makes significant contributions in Azpeitia/Urretxu (65–75%), in Bilbao this PAH makes only a moderate contribution (21%), with a value similar to that presented by IdP (19%). This PAH was also found to be relevant by BP86 calculations, but not by B3LYP/PBE0 computations. For Bilbao, the  $\omega$ B97XD functional predicted BaP as the main contributor (53%).

Having analyzed these findings, it is interesting to note that while calculations with different functionals show general agreement with the number and position of absorption bands, the relevance of each PAH can vary significantly.

Considering the most red-shifted absorption band provided by each functional (Tables S3, S5, S7, and S9), all calculations agree qualitatively that BaP, BghiP, and BkF provide relevant contributions. However, BP86 and  $\omega$ B97XD predict moderate contributions from IdP, while this PAH was found to be not relevant by PBE0 and B3LYP calculations. BaA is another PAH found to have nonnegligible contributions by some functionals (B3LYP and  $\omega$ B97XD) but not others (PBE0 and BP86). Finally, only PBE0 predicts relevant contributions from BbF in the visible region.

As for the more blue-shifted absorption bands in the UVA region (Tables S2, S4, S6, and S8), calculations with the four functionals agree on the relevance of the contributions made by BbF, PYR, and FLUO. Three functionals (B3LYP, PBE0, and  $\omega$ B97XD) also agree on the relevance of CHRY, with BP86 instead predicting contributions from IdP. Nevertheless, the level of agreement regarding individual contributions made by PAHs for the band at ~325–380 nm (depending on the functional used) appears to be greater than for the band at ~365/380–425 nm (once again, depending on the functional).

In conclusion, and despite some functional-dependent variability, these calculations agree that the studied PAHs should induce radiative forcing in the target Basque Country regions by light absorption at the “middle” of the UVA region and at short (sub)visible wavelengths. The potentially most problematic PAHs in the UVA region were found to be BbF, PYR, and FLUO, with some doubt regarding the importance of CHRY and IdP. As for the absorption at short (sub)visible wavelengths, BaP, BkF, and BghiP were consistently found to be problematic PAHs, while the contributions made by IdP, BaA, BghiP, and BbF to radiative forcing in this region require further study.

Finally, it should be noted that differences between the absorption spectra simulated in this work and those from the real world are expected. In the atmosphere, PAHs are susceptible to degradation and can be transformed into secondary organic aerosols (e.g., conversion of PAHs into oxygenated and nitrated derivatives). Furthermore, since we are working with mean atmospheric concentration values, and studies typically do not indicate the concentrations obtained for each measured sample, we are not able to model daily real-world absorption spectra. We are still at the beginning of the use of computational chemistry to model real-world absorption spectra of BrC, and studies of this sort show the intrinsic absorption properties of these PAHs at target sites. Moreover, if real-world spectra are obtained by other means, the differences between them and the models presented here can point to the processes that determine the light absorption of PAHs in the atmosphere.

#### 4. Conclusions

In this work, the real-world light absorption spectra of 14 PAHs over three regions of the Basque Country (Spain)—Azpeitia and Urretxu in the Gipuzkoa region and Bilbao—were modeled to identify the most significant absorption regions for PAH-induced radiative forcing. The theoretical absorption spectrum for each PAH at each sampling site was calculated using a TD-DFT approach with four density functionals, corrected with the experimental concentration, and the resulting data were combined to generate real-world absorption spectra.

Our results indicate that the combined absorption spectra of the PAHs over the different regions are qualitatively identical, with the main difference being the absorption intensity. More specifically, light absorption by PAHs appears to be more intense over Bilbao than in the Gipuzkoa region, meaning that the former should be subjected to more PAH-induced radiative forcing than the latter.

The theoretical calculations also indicate that PAH-induced radiative forcing over the studied regions should be limited to light absorption at the UVA and (sub)visible regions of the spectrum. Specifically, benzo[*b*]fluoranthene, pyrene, and fluoranthene were consistently found to be relevant for absorption at the UVA region, while some doubt about the relevance of chrysene and indeno[1,2,3-*cd*]pyrene remained. As for absorption at (sub)visible wavelengths, benzo[*a*]pyrene, benzo[*k*]fluoranthene, and benzoperylene were identified as problematic PAHs, while the magnitude of light absorption by indeno[1,2,3-*cd*]pyrene, benzo[*a*]anthracene, and benzo[*b*]fluoranthene still requires further study.

**Supplementary Materials:** The following are available online at <https://www.mdpi.com/article/10.3390/suschem2040033/s1>, Figure S1: Chemical structures of studied PAHs; Figure S2: Map showing location of sampling sites; Cartesian coordinates of naphthalene (NAP), phenanthrene (PHE), fluoranthene (FLUO), pyrene (PYR), benzo[*a*]anthracene (BaA), chrysene (CHR), benzo[*b*]fluoranthene (BbF), benzo[*k*]fluoranthene (BkF), benzo[*a*]pyrene (BaP), benzoperylene (BghiP), indeno[1,2,3-*cd*]pyrene (IdP), fluorene (FLU), dibenzo[*a,h*]anthracene (DahA), and anthracene (ANTH); Table S1: Experimental

mean concentration of PAHs over Azpeitia, Urretxu, and Bilbao; Table S2: Relative contribution (in %) of individual PAHs to absorption intensity at ~380 nm over Azpeitia, Urretxu, and Bilbao using BP86/6-31+G(d,p); Table S3: Relative contribution (in %) of individual PAHs to absorption intensity at ~425 nm over Azpeitia, Urretxu, and Bilbao using BP86/6-31+G(d,p); Table S4: Relative contribution (in %) of individual PAHs to absorption intensity at ~345 nm over Azpeitia, Urretxu, and Bilbao using PBE0/6-31G(d,p); Table S5: Relative contribution (in %) of individual PAHs to absorption intensity at ~400 nm over Azpeitia, Urretxu, and Bilbao using PBE0/6-31G(d,p); Table S6: Relative contribution (in %) of individual PAHs to absorption intensity at ~360 nm over Azpeitia, Urretxu, and Bilbao using B3LYP/6-31+G(d,p); Table S7: Relative contribution (in %) of individual PAHs to absorption intensity at ~410 nm over Azpeitia, Urretxu, and Bilbao using B3LYP/6-31+G(d,p); Table S8: Relative contribution (in %) of individual PAHs to absorption intensity at ~325 nm over Azpeitia, Urretxu, and Bilbao using wB97XD/6-31+G(d,p); Table S9: Relative contribution (in %) of individual PAHs to absorption intensity at ~365 nm over Azpeitia and Urretxu and ~382 nm over Bilbao using wB97XD/6-31+G(d,p); Table S10: Scope of selected datasets; Table S11: Summary of experimental datasets on which this study was based.

**Author Contributions:** Conceptualization, L.P.d.S.; Investigation, P.G.-B. and L.P.d.S.; writing—original draft preparation, P.G.-B.; writing—review and editing, P.G.-B. and L.P.d.S.; visualization, P.G.-B.; supervision, L.P.d.S.; funding acquisition, L.P.d.S. All authors have read and agreed to the published version of the manuscript.

**Funding:** This research was funded by projects UIDB/00081/2020 (CIQUP), UIDB/05748/2020 (GreenUPorto), and PTDC/QUI-QFI/2870/2020. Luís Pinto da Silva acknowledges funding from Fundação para a Ciência e Tecnologia (FCT, Portugal), under the Scientific Employment Stimulus (CEECIND/01425/2017). Patricia González-Berdullas acknowledges project PTDC/QUI-QFI/2870/2020 for funding her Post-Doc position.

**Acknowledgments:** The Laboratory of Computational Modelling of Environmental Pollutants–Human Interactions (LACOMEPhi) is acknowledged.

**Conflicts of Interest:** The authors declare no conflict of interest.

## References

1. Andreae, M.O.; Gelencser, A. Black carbon or brown carbon? The nature of light-absorbing carbonaceous aerosols. *Atmos. Chem. Phys.* **2006**, *6*, 3131–3148. [[CrossRef](#)]
2. Lei, Y.L.; Shen, Z.X.; Wang, Q.Y.; Zhang, T.; Cao, J.J.; Sun, J.; Zhang, Q.; Wang, L.Q.; Xu, H.M.; Tian, J.; et al. Optical characteristics and source apportionment of brown carbon in winter PM<sub>2.5</sub> over Yulin in Northern China. *Atmos. Res.* **2018**, *213*, 27–33. [[CrossRef](#)]
3. Lin, P.; Liu, J.; Shilling, J.E.; Kathmann, S.M.; Laskin, J.; Laskin, A. Molecular characterization of brown carbon (BrC) chromophores in secondary organic aerosol generated from photo-oxidation of toluene. *Phys. Chem. Chem. Phys.* **2015**, *17*, 23312–23325. [[CrossRef](#)] [[PubMed](#)]
4. Zhu, C.S.; Li, L.J.; Huang, H.; Dai, W.T.; Lei, Y.L.; Qu, Y.; Huang, R.J.; Wang, Q.Y.; Shen, Z.X.; Cao, J.J. n-Alkanes and PAHs in the Southeastern Tibetan Plateau: Characteristics and Correlations with Brown Carbon Light Absorption. *J. Geophys. Res. Atmos.* **2020**, *125*, e2020JD032666. [[CrossRef](#)]
5. Huang, R.J.; Yang, L.; Cao, J.; Chen, Y.; Chen, Q.; Li, Y.; Duan, J.; Zhu, C.; Dai, W.; Wang, K.; et al. Brown Carbon Aerosol in Urban Xi'an, Northwest China: The Composition and Light Absorption Properties. *Environ. Sci. Technol.* **2018**, *52*, 6825–6833. [[CrossRef](#)]
6. Lack, D.A.; Langridge, J.M.; Bahreini, R.; Cappa, C.D.; Middlebrook, A.M.; Schwarz, J.P. Brown carbon and internal mixing in biomass burning particles. *Proc. Natl. Acad. Sci. USA* **2012**, *109*, 14802–14807. [[CrossRef](#)] [[PubMed](#)]
7. Liu, J.; Bergin, M.; Guo, H.; King, L.; Kotra, N.; Edgerton, E.; Weber, R.J. Size-resolved measurements of brown carbon in water and methanol extracts and estimates of their contribution to ambient fine-particle light absorption. *Atmos. Chem. Phys.* **2013**, *13*, 12389–12404. [[CrossRef](#)]
8. Xu, J.; Cui, T.Q.; Fowler, B.; Fankhauser, A.; Yang, K.; Surratt, J.D.; McNeill, V.F. Aerosol Brown Carbon from Dark Reactions of Syringol in Aqueous Aerosol Mimics. *ACS Earth Space Chem.* **2018**, *2*, 608–617. [[CrossRef](#)]
9. Lin, G.X.; Penner, J.E.; Flanner, M.G.; Sillman, S.; Xu, L.; Zhou, C. Radiative forcing of organic aerosol in the atmosphere and on snow: Effects of SOA and brown carbon. *J. Geophys. Res.-Atmos.* **2014**, *119*, 7453–7476. [[CrossRef](#)]
10. Saleh, R.; Marks, M.; Heo, J.; Adams, P.J.; Donahue, N.M.; Robinson, A.L. Contribution of brown carbon and lensing to the direct radiative effect of carbonaceous aerosols from biomass and biofuel burning emissions. *J. Geophys. Res.-Atmos.* **2015**, *120*, 10285–10296. [[CrossRef](#)]
11. Frka, S.; Sala, M.; Kroflic, A.; Hus, M.; Cusak, A.; Grgic, I. Quantum Chemical Calculations Resolved Identification of Methylnitrocatechols in Atmospheric Aerosols. *Environ. Sci. Technol.* **2016**, *50*, 5526–5535. [[CrossRef](#)] [[PubMed](#)]

12. Chung, C.E.; Ramanathan, V.; Decremer, D. Observationally constrained estimates of carbonaceous aerosol radiative forcing. *Proc. Natl. Acad. Sci. USA* **2012**, *109*, 11624–11629. [[CrossRef](#)]
13. Lin, P.; Aiona, P.K.; Li, Y.; Shiraiwa, M.; Laskin, J.; Nizkorodov, S.A.; Laskin, A. Molecular Characterization of Brown Carbon in Biomass Burning Aerosol Particles. *Environ. Sci. Technol.* **2016**, *50*, 11815–11824. [[CrossRef](#)] [[PubMed](#)]
14. De Haan, D.O.; Tapavicza, E.; Riva, M.; Cui, T.; Surratt, J.D.; Smith, A.C.; Jordan, M.C.; Nilakantan, S.; Almodovar, M.; Stewart, T.N.; et al. Nitrogen-Containing, Light-Absorbing Oligomers Produced in Aerosol Particles Exposed to Methylglyoxal, Photolysis, and Cloud Cycling. *Environ. Sci. Technol.* **2018**, *52*, 4061–4071. [[CrossRef](#)]
15. Phillips, S.M.; Bellcross, A.D.; Smith, G.D. Light Absorption by Brown Carbon in the Southeastern United States is pH-dependent. *Environ. Sci. Technol.* **2017**, *51*, 6782–6790. [[CrossRef](#)] [[PubMed](#)]
16. Adler, G.; Wagner, N.L.; Lamb, K.D.; Manfred, K.M.; Schwarz, J.P.; Franchin, A.; Middlebrook, A.M.; Washenfelder, R.A.; Womack, C.C.; Yokelson, R.J.; et al. Evidence in biomass burning smoke for a light-absorbing aerosol with properties intermediate between brown and black carbon. *Aerosol Sci. Technol.* **2019**, *53*, 976–989. [[CrossRef](#)]
17. Cheng, Z.Z.; Atwi, K.M.; Yu, Z.H.; Avery, A.; Fortner, E.C.; Williams, L.; Majluf, F.; Krechmer, J.E.; Lambe, A.T.; Saleh, R. Evolution of the light-absorption properties of combustion brown carbon aerosols following reaction with nitrate radicals. *Aerosol Sci. Technol.* **2020**, *54*, 849–863. [[CrossRef](#)]
18. Cheng, Z.Z.; Atwi, K.; El Hajj, O.; Ijeli, I.; Al Fischer, D.; Smith, G.; Saleh, R. Discrepancies between brown carbon light-absorption properties retrieved from online and offline measurements. *Aerosol Sci. Technol.* **2021**, *55*, 92–103. [[CrossRef](#)]
19. d’Hendecourt, L.; Ehrenfreund, P. Spectroscopic properties of polycyclic aromatic hydrocarbons (PAHs) and astrophysical implications. *Adv. Space Res.* **1997**, *19*, 1023–1032. [[CrossRef](#)]
20. Cheng, Y.; He, K.B.; Engling, G.; Weber, R.; Liu, J.M.; Du, Z.Y.; Dong, S.P. Brown and black carbon in Beijing aerosol: Implications for the effects of brown coating on light absorption by black carbon. *Sci. Total Environ.* **2017**, *599–600*, 1047–1055. [[CrossRef](#)] [[PubMed](#)]
21. Denier van der Gon, H.; van het Bolscher, M.; Visschedijk, A.; Zandveld, P. Emissions of persistent organic pollutants and eight candidate POPs from UNECE–Europe in 2000, 2010 and 2020 and the emission reduction resulting from the implementation of the UNECE POP protocol. *Atmos. Environ.* **2007**, *41*, 9245–9261. [[CrossRef](#)]
22. Mari, M.; Harrison, R.M.; Schuhmacher, M.; Domingo, J.L.; Pongpiachan, S. Inferences over the sources and processes affecting polycyclic aromatic hydrocarbons in the atmosphere derived from measured data. *Sci. Total Environ.* **2010**, *408*, 2387–2393. [[CrossRef](#)] [[PubMed](#)]
23. Kim, B.M.; Lee, S.B.; Kim, J.Y.; Kim, S.; Seo, J.; Bae, G.N.; Lee, J.Y. A multivariate receptor modeling study of air-borne particulate PAHs: Regional contributions in a roadside environment. *Chemosphere* **2016**, *144*, 1270–1279. [[CrossRef](#)] [[PubMed](#)]
24. Fu, Z.; Wang, Y.; Chen, J.; Wang, Z.; Wang, X. How PBDEs Are Transformed into Dihydroxylated and Dioxin Metabolites Catalyzed by the Active Center of Cytochrome P450s: A DFT Study. *Environ. Sci. Technol.* **2016**, *50*, 8155–8163. [[CrossRef](#)]
25. Krzeminska, A.; Paneth, P. DFT Studies of SN2 Dechlorination of Polychlorinated Biphenyls. *Environ. Sci. Technol.* **2016**, *50*, 6293–6298. [[CrossRef](#)] [[PubMed](#)]
26. Pinto da Silva, L. Theoretical Study of the Ring-Opening of Epoxides Catalyzed by Boronic Acids and Pyridinic Bases. *J. Phys. Chem. C* **2017**, *121*, 16300–16307. [[CrossRef](#)]
27. Pinto da Silva, L. Mechanistic study of the role of hydrogen bond donors in the two-component organocatalysis of the ring-opening reaction of epoxides. *Mol. Catal.* **2019**, *474*, 110425. [[CrossRef](#)]
28. Adamo, C.; Jacquemin, D. The calculations of excited-state properties with Time-Dependent Density Functional Theory. *Chem. Soc. Rev.* **2013**, *42*, 845–856. [[CrossRef](#)] [[PubMed](#)]
29. Chen, J.Y.; Rodriguez, E.; Jiang, H.H.; Chen, K.P.; Frie, A.; Zhang, H.F.; Bahreini, R.; Lin, Y.H. Time-Dependent Density Functional Theory Investigation of the UV-Vis Spectra of Organonitrogen Chromophores in Brown Carbon. *ACS Earth Space Chem.* **2020**, *4*, 311–320. [[CrossRef](#)]
30. Hede, T.; Murugan, N.A.; Kongsted, J.; Leck, C.; Agren, H. Simulations of light absorption of carbon particles in nanoaerosol clusters. *J. Phys. Chem. A* **2014**, *118*, 1879–1886. [[CrossRef](#)]
31. Magalhães, A.C.O.; Esteves da Silva, J.C.G.; Pinto da Silva, L. Density Functional Theory Calculation of the Absorption Properties of Brown Carbon Chromophores Generated by Catechol Heterogeneous Ozonolysis. *ACS Earth Space Chem.* **2017**, *1*, 353–360. [[CrossRef](#)]
32. Dolomatov, M.Y.; Shutkova, S.A.; Bakhtizin, R.Z.; Dolomatova, M.M.; Latypov, K.F.; Gilmanshina, K.A.; Badretdinov, B.R. Structure of Asphaltene Molecules and Nanoclusters Based on Them. *Pet. Chem.* **2020**, *60*, 16–21. [[CrossRef](#)]
33. Elorduy, I.; Elcoroaristizabal, S.; Durana, N.; Garcia, J.A.; Alonso, L. Diurnal variation of particle-bound PAHs in an urban area of Spain using TD-GC/MS: Influence of meteorological parameters and emission sources. *Atmos. Environ.* **2016**, *138*, 87–98. [[CrossRef](#)]
34. Oleagoitia, M.B.Z.; Manterola, A.L.; Maurologoitia, J.I.; de Dicastillo, M.D.M.L.; Alvarez, J.; Barandiaran, M.A.; Loibide, A.I.; Santa-Marina, L. Polycyclic aromatic hydrocarbons (PAHs) in air associated with particles PM2.5 in the Basque Country (Spain). *Air Qual. Atmos. Health* **2019**, *12*, 107–114. [[CrossRef](#)]
35. Pinto da Silva, L.; Dias, T.B.; Esteves da Silva, J.C.G. Modelling the absorption spectra of polycyclic aromatic hydrocarbons over Seoul, South Korea. *Environ. Technol. Innov.* **2020**, *17*, 100536. [[CrossRef](#)]

36. Sousa, J.; Pinto da Silva, L. Modelling the absorption properties of polycyclic aromatic hydrocarbons and derivatives over three European cities by TD-DFT calculations. *Sci. Total Environ.* **2019**, *695*, 133881. [[CrossRef](#)] [[PubMed](#)]
37. Frisch, M.J.; Trucks, G.W.; Schlegel, H.B.; Scuseria, G.E.; Robb, M.A.; Cheeseman, J.R.; Scalmani, G.; Barone, V.; Mennucci, B.; Petersson, G.A.; et al. *Gaussian 09, Revision D.01*; Gaussian, Inc.: Wallingford, CT, USA, 2013.
38. Adamo, C.; Barone, V. Toward reliable density functional methods without adjustable parameters: The PBE0 model. *J. Chem. Phys.* **1999**, *110*, 6158–6170. [[CrossRef](#)]
39. Barone, V.; Cimino, P.; Crescenzi, O.; Pavone, M. Ab initio computation of spectroscopic parameters as a tool for the structural elucidation of organic systems. *J. Mol. Struct.* **2007**, *811*, 323–335. [[CrossRef](#)]
40. Jacquemin, D.; Preat, J.; Perpète, E.A.; Adamo, C. Absorption Spectra of Recently Synthesised Organic Dyes: A TD-DFT Study. *Int. J. Quantum Chem.* **2010**, *110*, 2121–2129. [[CrossRef](#)]
41. Le Bahers, T.; Adamo, C.; Ciofini, I. Photophysical properties of 8-hydroxyquinoline-5-sulfonic acid as a function of the pH: A TD-DFT investigation. *J. Phys. Chem. A* **2010**, *114*, 5932–5939. [[CrossRef](#)] [[PubMed](#)]
42. Pinto da Silva, L.; Esteves da Silva, J.C. Computational investigation of the effect of pH on the color of firefly bioluminescence by DFT. *ChemPhysChem* **2011**, *12*, 951–960. [[CrossRef](#)] [[PubMed](#)]
43. Becke, A.D. Density-functional thermochemistry. III. The role of exact exchange. *J. Chem. Phys.* **1993**, *98*, 5648–5652. [[CrossRef](#)]
44. Chai, J.D.; Head-Gordon, M. Long-range corrected hybrid density functionals with damped atom-atom dispersion corrections. *Phys. Chem. Chem. Phys.* **2008**, *10*, 6615–6620. [[CrossRef](#)]
45. Bruhn, T.; Schaumlöffel, A.; Hemberger, Y.; Bringmann, G. SpecDis: Quantifying the comparison of calculated and experimental electronic circular dichroism spectra. *Chirality* **2013**, *25*, 243–249. [[CrossRef](#)] [[PubMed](#)]
46. ASTM. ASTM, G173-03. In *Standard Tables for Reference Solar Spectral Irradiances: Direct Normal and Hemispherical on 37° Tilted Surface*; ASTM International: West Conshohocken, PA, USA, 2012.